THE JOURNAL OF PHYSICAL CHEMISTRY B

Article

pubs.acs.org/JPCB

Vibrational and Electronic Circular Dichroism of Dimethyl Mesobilirubins-XIIIα

Sergio Abbate,*[,†] France Lebon,[†] Giovanna Longhi,[†] Stefan E. Boiadjiev,[‡] and David A. Lightner[§]

[†]Dipartimento di Scienze Biomediche e Biotecnologie, Università di Brescia, 25123 Brescia, Italy

[‡]Department of Chemistry and Biochemistry, Medical University-Pleven, 1 St. Kliment Ohridski Street, 5800 Pleven, Bulgaria

[§]Department of Chemistry, University of Nevada, Reno, Nevada 89557-0020, United States

Supporting Information

ABSTRACT: The vibrational circular dichroism (VCD) spectra of ($\alpha R,\alpha' R$)-, ($\alpha S,\alpha' S$)-, ($\beta R,\beta' R$)-, and ($\beta S,\beta' S$)-dimethylmesobilirubin-XIIIα have been recorded in the range of 1800−900 cm^{-1} in $CDCl_3$ solution and in mixed DMSO-d_6/$CDCl_3$ solutions. Ab initio density functional theory (DFT) calculations predict IR vibrational absorption (VA) and VCD spectra in excellent to good correspondence with observed data. The same calculations confirmed the ridge-tile conformation that has been known for a long time. Assignment of vibrational normal modes (NMs) sheds light on the relative importance of local moieties and groups in determining conformational properties of the molecules, as well as their interaction with solvent molecules. Time-dependent DFT (TDDFT) calculations were also performed to provide an understanding of electronic circular dichroism (ECD) spectra and confirm the well-known interpretation based on the exciton model.

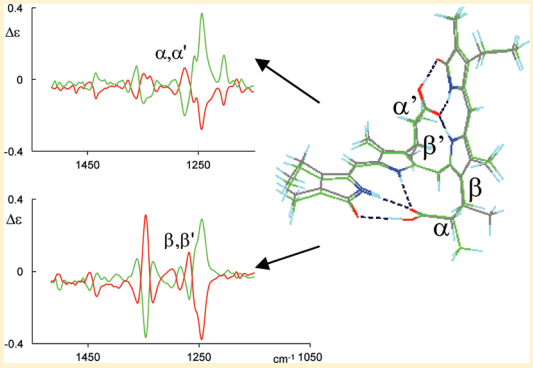

INTRODUCTION

Bilirubin is a yellow pigment produced following normal catabolism of heme in mammals.[1,2] It is insoluble in water, binds tightly to serum albumin, and is eliminated from circulation by acyl glucuronidation in the liver. Its accumulation in blood and extravascular tissues results in jaundice, which is often a useful indicator of liver disease. The conformation of bilirubin is reminiscent of a ridge-tile and was first observed in its crystals.[3,4] However, such a conformation is also stable in organic solvents and in water, as was observed by NMR spectroscopy.[5,6] In solution, circular dichroism (CD) in the UV−visible region, also referred to as electronic circular dichroism (ECD), has proven quite useful in providing simple verification of the ridge-tile conformation. Indeed, the simple interpretation[7] of the observed intense bisignate Cotton effects for bilirubin and mesobilirubin in the presence of human serum albumin or quinine[8] and many other chiral discriminators, on the basis of the exciton model, has provided a vivid almost-direct picture of the bilirubin molecule. Also, chiral derivatives of mesobilirubin with stereogenic centers, for example, ($\beta R,\beta' R$)-dimethylmesobilirubin-XIIIα, have been used successfully to investigate conformational properties and conformational changes in solution.[9,10] The same exciton system detected by induced CD of bilirubin, as observed in refs 7 and 8, was also found in natural ECD of their chiral derivatives described in refs 9 and 10, and changes in the CD spectra were then used as indicators of conformational change occurring in most bilirubin systems.

Vibrational circular dichroism (VCD) has been applied in conformational analyses for more than 30 years, and for 20 years, it has been used in conjunction with ab initio calculations, particularly density functional theory (DFT) calculations.[11,12] The concerted use of theory and experiments has solved intricate assignment problems in the field of natural products[13,14] and has also helped to better define conformational properties.[15,16] Important experimental VCD studies were presented by Urbanová et al.[17−19] dealing with bilirubin and biliverdin in the presence of chiral molecules. Ab initio studies of bilirubin[20,21] encompassing Hartree−Fock and DFT theories, molecular dynamics (MD) calculations, and polarizable continuum model (PCM) theory were applied in investigating its complicated conformational landscape, thereby leading to the proposal of mechanisms for solvating excited-state conformers. A yet more recent DFT calculation[22] dealt with the relationship between conformational properties and NMR parameters.

In the present work, we present investigations of ($\alpha R,\alpha' R$)-, ($\alpha S,\alpha' S$)-, ($\beta R,\beta' R$)-, ($\beta S,\beta' S$)-dimethylmesobilirubin-XIIIα by VCD in the mid-infrared range with the following aims: (1) to determine whether the main VCD features and calculated DFT geometrical properties of these chiral derivatives of mesobilirubin are similar to the VCD features of bilirubin in presence of chiral molecules,[17−19] as happens with ECD;[8−10] (2) to

Received: February 9, 2012
Revised: March 22, 2012
Published: April 13, 2012

   dx.doi.org/10.1021/jp3013255 | J. Phys. Chem. B 2012, 116, 5628−5636

investigate whether local changes at the bilirubin periphery, namely, changes in the methyl substitutions from α to β positions on the propionic acid chains, produce well-defined (even if minor) changes in the VCD spectra; (3) to determine whether DFT calculations once again allow characterization of the ridge-tile conformation of bilirubin systems and attribution of the main VCD and VA peaks to well-defined normal modes (NMs), thereby defining the relative importance of each molecular moiety in stabilizing the conformation or, conversely, in promoting destabilization; and (4) to take advantage of the observation that VCD chromophores have a local character,[11−13] as opposed to the global character of ECD chromophores.[7] That is, for objective 4, as for objective 2, we endeavored to use changes in individual VCD and IR bands to understand local changes in given parts of the molecules, caused by perturbations in the local environment that lead to global alterations in the pigment molecular conformation. Here, the particular interest lies with variations due to possible solvent-induced differences, especially between chloroform and dimethyl sulfoxide (DMSO) solvents.

EXPERIMENTAL AND COMPUTATIONAL DETAILS

The synthesis of the four optically active compounds under study is described in refs 23 and 24. [In Scheme 1, we report the (*R*,*R*) enantiomer of (α,α') as structure **1** and the (*R*,*R*)-enantiomer of (β,β') as structure **2**.] They were prepared in 100% enantiomeric excess. The VCD spectra were obtained with a JASCO FVS4000 FTIR spectrometer equipped with a VCD module and with a mercury cadmium telluride (MCT) detector. A 0.018 M $CDCl_3$ solution for **2** and a 0.016 or 0.015 M solution for **1** were prepared, and all spectra were recorded with samples in 100-μm-path-length cells (BaF_2 windows); the reported spectra are averages over four sets of 2000 spectra each, with 4 cm^{-1} resolution. VCD spectra in mixed solvents were obtained on similarly concentrated solutions, dissolving **1** and **2** in $CDCl_3$/DMSO-d_6 mixtures with increasing DMSO concentration so as to match the percentages (v/v) reported in the figures. All reported spectra have had the solvent spectrum subtracted. ECD spectra were obtained on a JASCO 815SE spectrometer with 2-nm resolution, with four scans and 0.001 M solutions.

Scheme 1

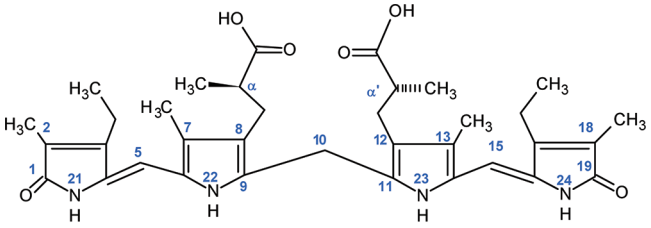

1:(αR,α'R)-Dimethylmesobilirubin-XIIIα

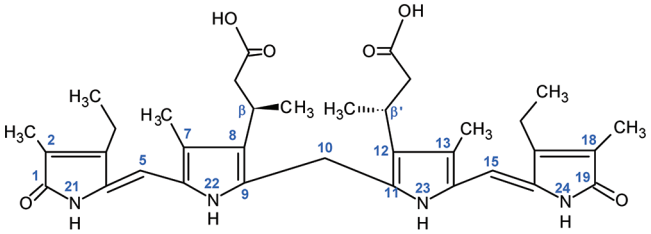

2: (βR,β'R)-Dimethylmesobilirubin-XIIIα

RESULTS AND DISCUSSION

In Figure 1, we show superimposed the calculated DFT structures of (αS,$\alpha' S$)- and (βS,$\beta' S$)-dimethylmesobilirubin-XIIIα, obtained by minimizing the preliminary structures defined by semiempirical methods. The ridge-tile-type structure found here was confirmed previously and is widely accepted in the literature. Changes from the conformations of Figure 1 are with the ethyl groups in the lactam moiety, where their methyls are rotated by ca. ±90° about the C—C bond connecting the ethyl to the lactam. Similar energies were found in this case,

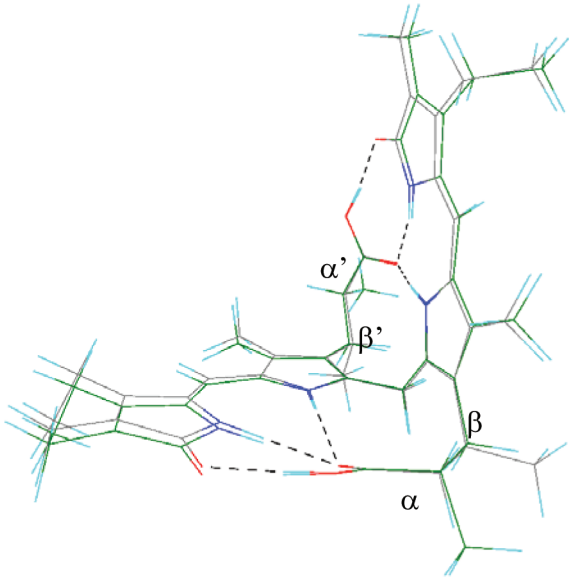

Figure 1. Superimposed calculated structures of (αS,$\alpha' S$)- and (βS,$\beta' S$)-dimethylmesobilirubin-XIIIα (green and gray traces, respectively). DFT calculations based on Gaussian 2009[25] with the B3LYP/TZVP functional/basis set.

dx.doi.org/10.1021/jp3013255 | J. Phys. Chem. B 2012, 116, 5628−5636

Table 1. DFT-Calculated Values for Selected Geometrical Parameters of (αS,α′S)- and (βS,β′S)-Dimethylmesobilirubin-XIIIα in Vacuo[a] and Comparison with Calculated and Experimental Values from the Literature on Bilirubin[b]

	(αS,α′S) DFT	(βS,β′S) DFT	Bili H−F[21]	Bili H−F[22]	MD SYBYL[8]	X-ray[3]	X-ray[4]
ϕ_1(22−9−10−11) (deg)	−61.1	−59.4	62	–	−59.1	−59.8	−63.3
ϕ_2(23−11−10−9) (deg)	−61.1	−59.4	62	–	−58.9	−63.7	−60.6
θ (2−8−12−18) (deg)	−102.3	−95.8	–	–	85	97	97
O—H···O═ (Å)	1.625	1.631	–	1.61	1.55	1.58	1.49
N_{lactam}—H···O═ (Å)	1.841	1.812	–	1.81	1.56	1.70	1.77
N_{pyrrol}—H···O═ (Å)	1.978	1.983	–	1.95	1.56	1.81	1.90

[a]For atomic numbering defining ϕ_1, ϕ_2, and θ angles, see Scheme 1. [b]Also see the text.

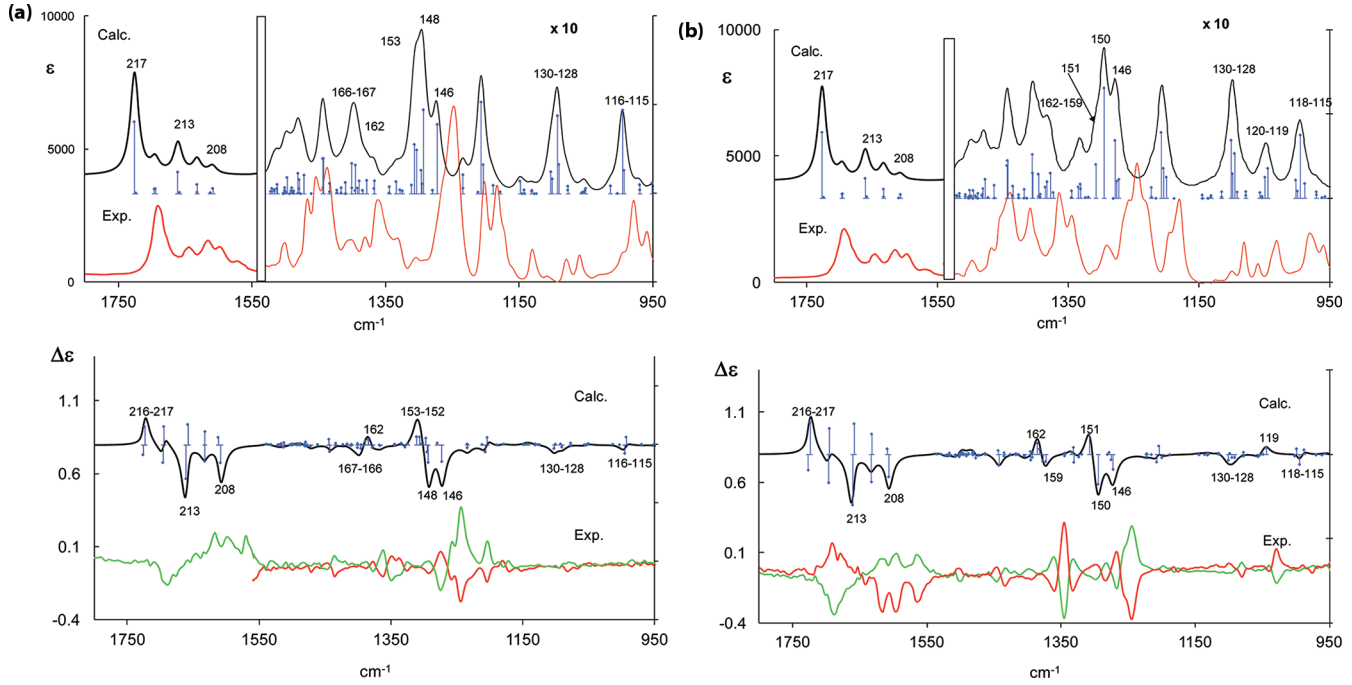

Figure 2. Comparison of experimental IR-VA (top) and VCD (bottom) of (a) (αR,α′R)- and (αS,α′S)-dimethylmesobilirubin-XIIIα (green and red traces, respectively) and (b) (βR,β′R)- and (βS,β′S)-dimethylmesobilirubin-XIIIα (green and red traces, respectively) with the corresponding calculated spectra of (a) (αS,α′S)-dimethylmesobilirubin-XIIIα and (b) (βS,β′S)-dimethylmesobilirubin-XIIIα in vacuo (B3LYP/TZVP). In both cases, inside the calculated VA and VCD bands, we report, at the calculated frequencies, bars whose heights are proportional to the calculated dipole and rotational strengths, respectively. Numbers close to bars refer to calculated normal modes defined by Gaussian.

and the calculated spectra are almost superimposable; in Figure 2 below, we report calculated spectra of the lower-energy conformation, for which the two ethyls point outward with respect to the ridge-tile structure. As reported several times previously for the mesobilirubins,[8] the (S,S) configuration promotes the M helicity of the ridge-tile conformation of the molecules. In Figures SI-1 and SI-2 of the Supporting Information, we report also the secondary P minima, calculated with the present DFT approach. They are not just "mirror images" of the M minima. We also present in the Supporting Information the value for the energy difference between the global and local minima. To better evaluate the geometry of the molecule, we report in Table 1 the values of a few selected parameters that we evaluated starting from Figure 1 and compare them with the corresponding data in the literature. Comparison with previous calculations and X-ray diffraction data is very good. One can also note that the (βS,β′S)-dimethylmesobilirubin-XIIIα is slightly more closed than the corresponding (αS,α′S) molecule, as manifested by the parameters for the θ(2−8−12−18) torsion angle and the N_{lactam}—H···O═C distance. Despite the minuscule difference, this prediction is fairly safe and appears to be due to the CH_3 groups in the (βS,β′S) compound being farther from the COOH groups involved in the three hydrogen bonds that stabilize the ridge-tile conformation.

In Figure 2, we report comparisons of experimental VA and VCD spectra for (αR,α′R)-, (αS,α′S)-, (βR,β′R)-, and (βS,β′S)-dimethylmesobilirubin-XIIIα with the corresponding calculated spectra of (αS,α′S)- and (βS,β′S)-dimethylmesobilirubin-XIIIα, respectively. The experimental spectra for (αS,α′S)-dimethylmesobilirubin-XIIIα are not complete because of the limited availability of the compound. Acceptable to excellent mirror-image bands are observed in the VCD spectra of the (S,S) and (R,R) enantiomeric couples. Moreover, the present spectra compare reasonably well with the previous VCD and VA spectra of bilirubin in refs 17−19 but now span over a larger frequency range and are not superimposed onto signals from the chiral complexing agents, for example, polypeptides and cyclodextrins. The experimental VCD spectra contain fairly intense VCD features, reaching values for g close to 10^{-3} for bands around 1350 and 1250 cm^{-1}. Note that the lower-frequency region of the VA spectra has been multiplied by 10;

dx.doi.org/10.1021/jp3013255 | J. Phys. Chem. B 2012, 116, 5628−5636

Table 2. Comparison of the Wavenumbers for the Observed IR-VA and VCD Bands for (αR,α′R)- and of (βR,β′R)-Dimethylmesobilirubin-XIIIα, Together with a Rough Assignment Based on Visual Inspection of GaussView[25] for Selected Features, and Frequencies of the Bands Observed by Resonance Raman Spectroscopy on (αR,α′R)-Dimethylmesobilirubin-XIIIα Performed in Ref 33

αR,α′R				βR,β′R		
assignment[a]	VCD[b]	IR	Raman[33]	VCD[b]	IR	assignment[a]
C═Os + OHb + NHb	1693 (−)	1691		1691 (−)	1693	C═Os + OHb + NHb
		1645	1648	1642 (+)	1646	
NHb(la)	1618 (+)	1616		1616 (+)	1615	NHb(la)
	1600 (+)	1598	1603	1596 (+)	1598	
NHb(py)	1571 (+)	1572	1581 sh	1565 (+)	1569	NHb(py)
		1502	1506	1495 (+)	1496	
		1466	← →	1471 (+)	1468	
	1455 (−)	1453	1458	1447 (−)	1454 (sh)	
	1437 (+)	1439	← sh →	1435 (+)	1439	
	1396 (+)	1402	1408	1406 (+) broad	1408	
	1379 (−)	1381				
C*Hb + NHb	1364 (+)	1362	1367	1361 (+)	1363	C*Hb + NH/OHb
	1352 (−)					
C*Hb + NH/OHb	1327 (+)	1332	1343	1345 (−)	1344 + 1333 (sh)	C*Hb + NH/OHb
	1299 (+)			1332 (+)		
C*Hb + CH_2w	1276 (−)	1304	1313	1297 (−)	1292	C*Hb + CH_2w
			1293	1283 (+)		
C*Hb + CH_2w	1245 (+)	1247	1278	1267 (−)	1259 (sh) + 1244	C*Hb + CH_2w
			1261	1244 (+)		
C*Hb + CH_2w	1204 (+)	1202		1198 (+)	1195	
	1182 (+?)	1183	1194	1172 (−)	1179	
		1131	broad feature	broad	1124	
			broad feature	1102 (−)	1098	
	1082 (+)	1078	broad feature	1079 (+)	1080	
	1066 (+)					
		1059	broad feature	1068 (−) broad	1059	
	988 (+)	998 (sh)	broad feature	1039 (+)	1037 (sh) + 1031	
				1028 (−)		
	976 (?)	978	979	989 (−)	981	
				976 (+)		
	957 (?)	960	959	963 (+)	958	

[a]s = stretching, b = bending, w = wagging, la = lactam, py = pyrrole. [b]Signs for VCD bands reported in parentheses.

however, the high-frequency region is intrinsically more intense because of the presence of the large-dipole-moment C═O stretching vibrations. This has been observed in another instance of a two-bladed C_2-biaziridinic compounds.[15] Clear, even though not major, differences in the VA data and especially in the VCD data between 1400 and 1200 cm^{-1} can be noticed between **1** (α,α′) and **2** (β,β′). We believe that this is due to the structural differences predicted by DFT calculations and noted above; in particular, we believe that the different positions of the methyls (either α or β) change the normal-mode patterns. In fact, however, the calculations are quite satisfactory except for the intense triplet of VCD features with alternating signs observed at ca. 1350 cm^{-1} for (βR,β′R)- and (βS,β′S)-dimethylmesobilirubin-XIIIα: indeed, the latter feature was calculated at an intensity that was too low. The calculated spectra allow the absolute configuration assignment to be confirmed. Most (but not all) calculated features come in pairs with quite different VA intensities and VCD bands that are almost equal in intensity and oppositely signed. (The bars in Figure 2 represent dipole and rotational strengths.) Inspection of the normal modes (NMs) shows that they are symmetric and antisymmetric combinations of fairly localized group modes resident in the two halves of the molecules and resembling vibrational excitons. (We note that the importance of exciton chirality in mid-IR VCD has been evidenced recently by Taniguchi and Monde, *J. Am. Chem. Soc.* **2012**, *134*, 3695−3698.) If one considers in particular the quite intense features between 1550 and 1750 cm^{-1}, one can clearly notice that antisymmetric modes show dipole derivatives perpendicular to the C_2 pseudosymmetry axis and exhibit at the same time large dipole strengths; in contrast, symmetric modes bear generally small dipole strengths and larger rotational strengths than antisymmetric modes. In most cases, though, the two opposite features of the excitons are not resolved, because they are too close in frequency, and the observed features are due to the overlap of the + and − components of the excitonic couplet, which are not equal in absolute value. The VCD bands above 1650 cm^{-1} are attributed to C═O stretching NM, which are also coupled to the bending of the N—H bond in the lactam moiety (see Table 2 and Tables SI-1 and SI-2 of the Supporting Information). The latter NH in-plane bending contributes to the intense VCD bands with opposite sign between 1650 and 1550 cm^{-1}, and the aspects of the whole region between 1700 and 1550 cm^{-1} are fairly similar in the calculated and experimental spectra of the (α,α′) and (β,β′) molecules. In contrast, the spectroscopic differences observed between (α,α′)

dx.doi.org/10.1021/jp3013255 | J. Phys. Chem. B 2012, 116, 5628−5636

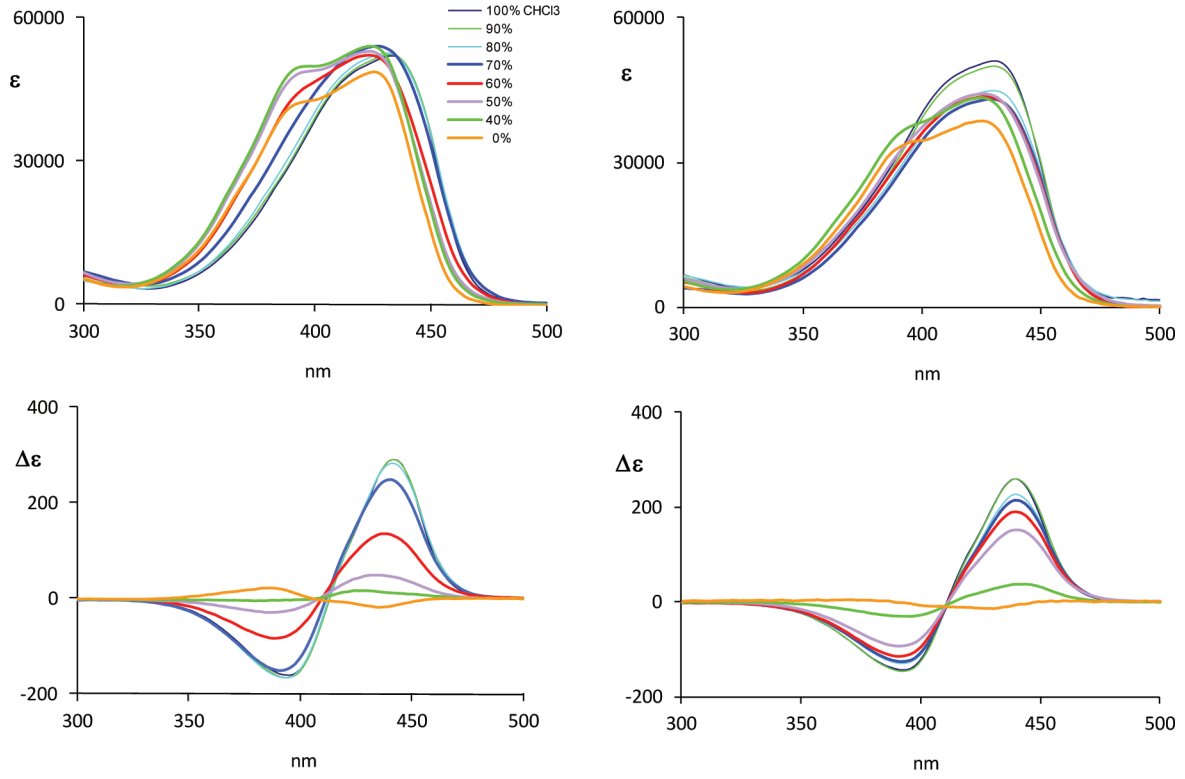

Figure 3. Experimental UV absorption (top) and ECD (bottom) spectra of (left) ($\alpha R,\alpha' R$)- and (right) ($\beta R,\beta' R$)-dimethylmesobilirubin-XIIIα in $CHCl_3$ and DMSO mixtures (volume percentages indicated in the legend).

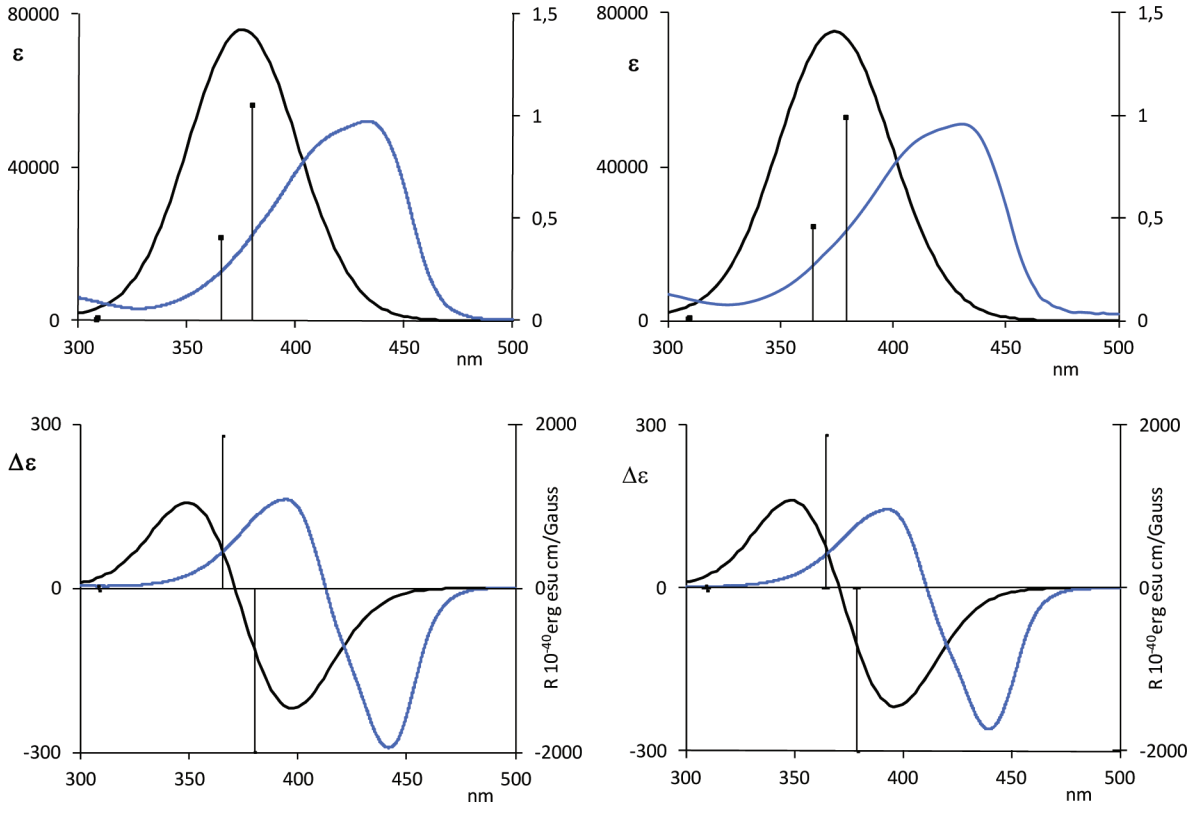

Figure 4. Comparison of calculated UV (top) and ECD spectra (bottom) of (left) ($\alpha S,\alpha' S$)- and (right) ($\beta S,\beta' S$)-dimethylmesobilirubin-XIIIα in vacuo (black traces) with the corresponding experimental spectra in chloroform solutions (blue traces). Bandwidths for the bands attributed to calculated transitions were 0.2 eV; the bars reported underneath the calculated bands are proportional to the calculated rotational or dipole strengths. For other information on calculations or experiments, see text.

dx.doi.org/10.1021/jp3013255 | J. Phys. Chem. B 2012, 116, 5628−5636

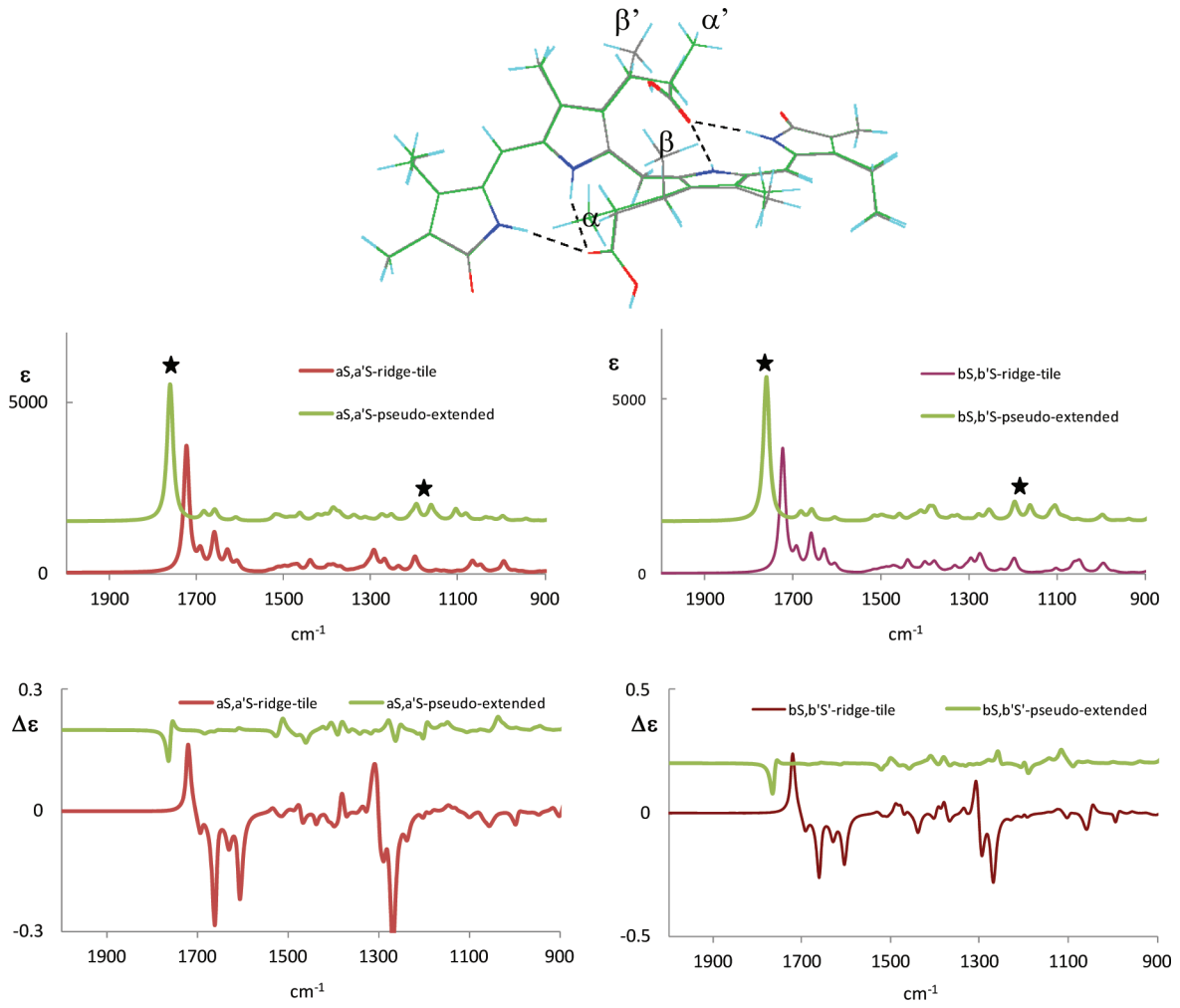

Figure 5. Top: Superimposed pseudoextended structures for (green) ($\alpha S,\alpha' S$)- and (gray) ($\beta S,\beta' S$)-dimethylmesobilirubin-XIIIα conformations obtained by DFT calculations in vacuo. Bottom: DFT-calculated IR and VCD spectra of (left) ($\alpha S,\alpha' S$)- and (right) ($\beta S,\beta' S$)-dimethylmesobilirubin-XIIIα for both the ridge-tile and pseudoextended conformations.

and (β,β') for the features at ca. 1350 cm^{-1} are attributed to the NM involving mostly bending of the C*H bond coupled to NH in-plane bending (either for the pyrrole or the lactam), to OH bending, and finally to CH_2 wagging modes of nearby units. Some differences between the (α,α') and (β,β') molecules are observed also in the VCD and IR intense region at ca. 1250 cm^{-1}, but they are not as important as those at ca. 1350 cm^{-1}. From the NM analysis, one can notice that contributions from C*H bending are still present, but they are coupled much more to CH_2 wagging modes rather than to NH in-plane bending modes.

In Figure 3, we report the ECD spectra of ($\alpha R,\alpha' R$)- and ($\beta S,\beta' S$)-dimethylmesobilirubin-XIIIα in $CHCl_3$ and in mixed $CHCl_3$/DMSO solutions. We observe that the differences between the ECD spectra of the (α,α') and (β,β') molecules are not as evident as in VCD, and this demonstrates once again how the latter technique can reveal specific local phenomena. With addition of DMSO, one can first notice a decrease in the $\Delta\varepsilon$ values of the ECD maxima of the excitonic features; at percentages of DMSO larger than ca. 60%, one can also notice that the UV components get farther apart in wavelengths, and at the same time, the $\Delta\varepsilon$ values of the ECD maxima decrease dramatically, changing sign at 100% DMSO. An exciton mechanism, as reported in refs 7, 9, and 10, for example, was shown to satisfactorily explain the ECD data. By the recently introduced TDDFT computational procedure, one is able to show that the exciton picture is correct. Indeed, in Figure 4, one can see first that the experimental ECD spectra are well reproduced by the TDDFT-calculated spectra (and the UV spectra as well), except for the overestimate of electronic transition frequencies; second, one learns that the observed large ECD couplet is due to just two transitions with large and opposite rotational strengths (in the figure, the latter are proportional to the bars underneath the bands); the corresponding wide UV band is instead due mostly to one of the two $\pi \rightarrow \pi^*$ transitions, the other bearing weaker dipole strength. Thus, the ECD spectrum, which had been previously and fruitfully interpreted in terms of an exciton couplet from dipyrrinone chromophores,[9,10] is now reconfirmed at the ab initio level. Moreover, on the basis of our calculations, the states associated with the relevant transitions are [(HOMO − 1 → LUMO + 1) + (HOMO → LUMO)] and [(HOMO − 1 → LUMO) + (HOMO → LUMO + 1)] (see Figure SI-3, Supporting Information).

The very striking effect on the ECD spectrum due to DMSO added to the solutions of ($\alpha R,\alpha' R$)- and ($\beta S,\beta' S$)-dimethylmesobilirubin-XIIIα in $CHCl_3$ (Figure 3) clearly suggests a reorientation of the dipyrrinones themselves. Their relative

dx.doi.org/10.1021/jp3013255 | J. Phys. Chem. B 2012, 116, 5628−5636

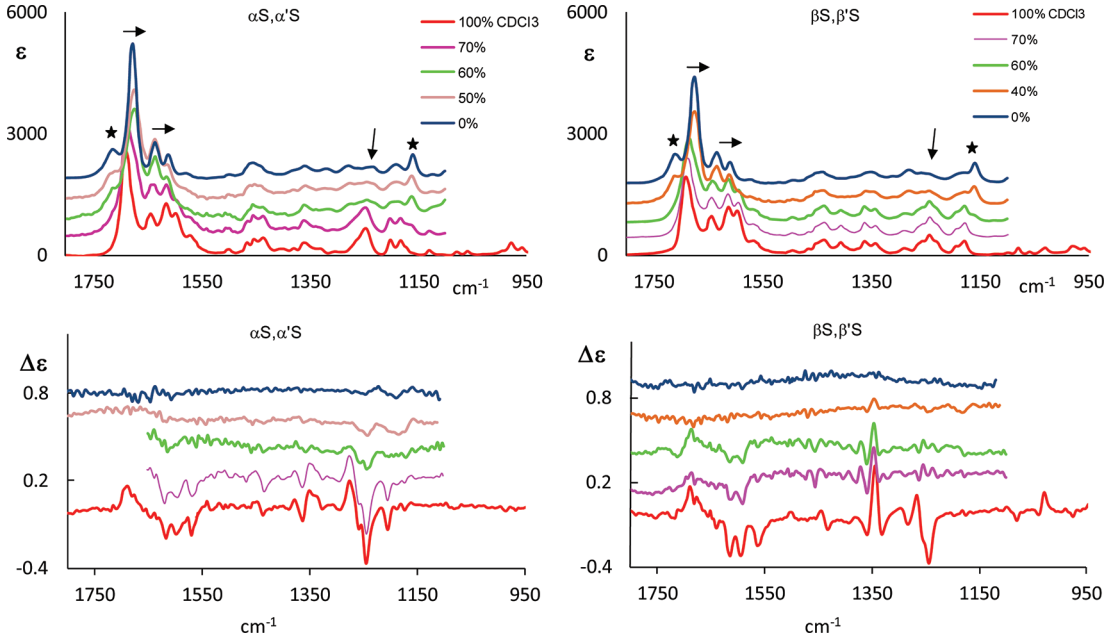

Figure 6. Experimental IR-VA (top) and VCD (bottom) of (left) (*αS,α′S*)- and (right) (*βS,β′S*)-dimethylmesobilirubin-XIII*α* in different $CDCl_3$/DMSO-d_6 mixtures (volume percentages indicated in the legends).

orientation is governed by their ability to rotate about the central CH_2 group to which they are conjoined, with limitations imposed by intramolecular hydrogen bonds. It is thus evident that the energetically most stable ridge-tile intramolecularly hydrogen-bonded conformation of the pigment in $CHCl_3$ solvent (and even in liquid crystals[30]) is someway perturbed by added DMSO. Yet one must not necessarily interpret a large change in the ECD as being due to a large change in conformation. Indeed, the T_1 NMR studies in pure DMSO led Kaplan and Navon[5] to the assessment that bilirubin adopted some sort of ridge-tile shape, a conformation where the propionic acid residues are immobilized still by hydrogen bonds, in which the solvent (DMSO) participates: "From the slowness of the internal motion of the propionic acid residues of bilirubin... it is concluded that these residues are tied to the skeleton via bound solvent molecules."[31] To accommodate this interpretation, the dihedral angle of the ridge-tile must open somewhat (to a more obtuse ridge-tile). This change reorients the relevant electronic transition moments of the two dipyrrinone chromophores from skewed toward "in-line", that is, a flatter pseudoextended structure.[8] In Figure SI-4 of the Supporting Information, we provide CAMB3LYP/TZVP-calculated ECD and UV spectra for a possible pseudoextended structure of (*αS,α′S*)- and of (*βS,β′S*)-dimethylmesobilirubin-XIII*α* as obtained by optimization in vacuo: this conformation is not one of those noted in ref 8 but encompasses four intramolecular NH···O═C hydrogen bonds. The corresponding calculated ECD spectra are not much less intense than those for the ridge-tile conformers, but show inverted signs in the two main bands and thus a likely inverted exciton behavior. The same exciton inversion was predicted to occur at about 120° torsional angles $\phi_1(22-9-10-11) = \phi_2(23-11-10-9)$ on the basis of molecular mechanics (MM) calculations.[8] The geometrical parameters of this new structure are given in Table SI-3 of the Supporting Information; a picture of this conformation is given in Figure 5, top panel, where we superimpose (*αS,α′S*) and (*βS,β′S*)-dimethylmesobilirubin-XIII*α*. At this point, we note that, in ref 8, MM-type calculations of bilirubin-type molecules reveal many different conformational structures of widely varying total energy, and we have no cogent a priori reason to argue that the pseudoextended conformers of Figure 5 predominate in DMSO solutions.

We now discuss whether the VCD data are not in contradiction with the existence of this conformation in solution. Indeed, we also recorded the VCD and IR-VA spectra for a few selected cases of mixed $CDCl_3$/DMSO-d_6 solutions examined by ECD (Figure 6). For the sake of clarity, we present results for the (*S*) enantiomer for both (*α,α′*)- and (*β,β′*)-dimethylmesobilirubin-XIII*α*: however, in the (*α,α′*) case, VCD spectra were recorded on (*αR,α′R*)-dimethylmesobilirubin-XIII*α* and were later inverted. Regarding the VCD spectra, we noticed that the major changes take place in the rather crucial 1350−1250 cm^{-1} interval, especially close to 1250 cm^{-1}, whereas in the carbonyl stretching region, changes in the VCD spectra are less pronounced. For 100% DMSO, no significant VCD feature was observed, within the limits of our instrumentation and of the concentration/cell used, but also the IR-VA spectrum was strongly perturbed. From a detailed analysis, one can observe the following: (i) The strongest IR carbonyl stretching band at ca. 1700 cm^{-1} is red-shifted; on the higher-frequency side of the latter band (at ca. 1730 cm^{-1}), a new distinct IR feature grows in, whereas on the lower-frequency side (at ca. 1600 cm^{-1}), the IR spectrum reduces to just two bands; the corresponding VCD features become progressively less and less intense with increasing DMSO content and change shape, until they disappear at ca. 60% DMSO concentration. (ii) At ca. 1350 cm^{-1}, the IR-VA features become less structured and weaker, possibly due to broadening, with increased DMSO content; correspondingly, the VCD features decrease in intensity and disappear above 40−50% DMSO concentration. (iii) At ca. 1250 cm^{-1}, there is a marked decrease in the IR feature with increased DMSO content, whereas the corresponding VCD features decrease in a less evident way with respect to what happens in the region close to 1350 cm^{-1}, disappearing at about 60% DMSO concentration.

dx.doi.org/10.1021/jp3013255 | J. Phys. Chem. B 2012, 116, 5628−5636

(iv) Finally, at ca. 1150 cm^{-1}, a new IR band grows in, possibly accompanied by the growing of a slightly less evident negative VCD band. The observed progressive changes in the 1350−1250 cm^{-1} VCD features take place with lower content of DMSO with respect to other spectroscopic regions, and particularly in the carbonyl C═O region, probably prior to solvent insertion into intramolecular hydrogen bonds. One learns from Table 2 that this region contains large contributions from C*H bending modes, and we believe that the latter signals are the modes sensitive to stereogenic changes. To further understand these changes, we also performed calculations of VCD spectra of (*αS,α′S*)- and of (*βS,β′S*)-dimethylmesobilirubin-XIII*α* for both pseudoextended conformers, to be compared with the ridge-tile conformers. The calculated IR and VCD spectra are reported in the lower panels of Figure 5. To establish whether the pseudoextended conformer is a plausible conformer that can be found in DMSO solution, we consider how the VCD and IR features are predicted vis-à-vis the experimental results of Figure 6. (i) The strong IR feature at 1720 cm^{-1} is calculated at too high a frequency with respect to the main IR band in that region, but could well correspond to the lower-intensity feature observed at ca. 1730 cm^{-1} (indicated by an asterisk in Figures 5 and 6). (ii, iii) At 1350 and 1250 cm^{-1}, the calculated IR features are much less intense than those for the ridge-tile conformer. (iv) On the contrary, at 1150 cm^{-1}, the calculated IR features for the pseudoextended conformer are more intense than those for the ridge-tile conformer (indicated by an asterisk in Figures 5 and 6). In all cases, the VCD calculated bands are weak, and it is hard to find a trace of any of them in the observed spectra. From this result, we can conclude that pseudoextended structures survive in DMSO and their spectroscopic signatures are identified, but some other structures might be present, the spectroscopic chiral features of which mutually cancel. This conclusion follows from only a preliminary investigation; to define the most probable conformations of dimethylmesobilirubins, DMSO should be treated as an explicit solvent (see ref 32). This will be the subject of a future study.

CONCLUSIONS

The VCD spectra of (*αR,α′R*)-, (*αS,α′S*)-, (*βR,β′R*)-, and (*βS,β′S*)-dimethylmesobilirubin-XIII*α* have been recorded for solutions in pure $CDCl_3$, in DMSO-d_6, and in mixtures of the two solvents. DFT calculations allow a satisfactory prediction of the IR-VA and VCD spectra of the two enantiomeric couples in $CDCl_3$. In the latter solvent, a small difference between the (*α,α′*) and (*β,β′*) molecules is noticed for some features at ca. 1350 cm^{-1}, corresponding to normal modes with contributions from bending of the C*H bond originating from the stereogenic carbon atoms. These same bands are also more sensitive to progressive addition of DMSO-d_6 to $CDCl_3$ solvent, causing progressive modification of the tight network of intramolecular hydrogen bonds that leads to a change of conformation, accompanied by dramatic changes in the VCD spectra. DFT calculations show how the ridge-tile conformation generates intense VCD bands both in the high-frequency region above 1550 cm^{-1} and, unusually, also in the region 1250−1350 cm^{-1}.

More extended conformations, such as that proposed here, preserving four of six intramolecular hydrogen bonds, exhibit quite small VCD intensities. Most importantly, new IR absorption observed in solutions containing DMSO were also correctly predicted; however, from a comparison of our calculations with experimental VA and VCD data, we are led to conclude that this sort of conformer is not the only one present.

The ECD spectra in $CHCl_3$ solution were newly interpreted in terms of TDDFT calculations assuming the ridge-tile conformation and were found to agree with the previous conclusions based on the exciton model for coupling dipyrrinone chromophores' $\pi \rightarrow \pi^*$ transitions. The same calculations for the pseudoextended conformer justify the sign inversion in both components of the UV CD couplet at 100% DMSO concentration: the fact that higher absolute intensities are calculated than experimentally observed leads us once more to conclude that the pseudoextended conformer might not be the only conformer in DMSO solution.

ASSOCIATED CONTENT

Supporting Information

M and P conformations of (*αS,α′S*)- and (*βS,β′S*)-dimethylmesobilirubin-XIII*α* obtained by DFT optimization (Figure SI-1 and SI-2, respectively). Calculated frequencies, dipole strengths, and rotational strengths and NM assignments of (*αS,α′S*)- and (*βS,β′S*)-dimethylmesobilirubin-XIII*α* (Tables SI-1 and SI-2, respectively). Calculated geometrical parameters of (*αS,α′S*)- and (*βS,β′S*)-dimethylmesobilirubin-XIII*α* in the ridge-tile and pseudoextended conformations (Table SI-3; for definition of parameters, see Scheme 1). Views of the two highest occupied and two lowest unoccupied molecular orbitals of (*αS,α′S*)-dimethylmesobirilubin XIII*α*: (a) HOMO − 1, (b) HOMO, (c) LUMO, and (d) LUMO + 1 (Figure SI-3). Calculated UV and ECD spectra of (*αS,α′S*)- and (*βS,β′S*)-dimethylmesobilirubin-XIII*α* (Figure SI-4A,B, respectively) for the ridge-tile and pseudoextended conformations. This material is available free of charge via the Internet at http://pubs.acs.org.

AUTHOR INFORMATION

Corresponding Author

*E-mail: abbate@med.unibs.it.

Notes

The authors declare no competing financial interest.

ACKNOWLEDGMENTS

G.L. is grateful to the Italian Ministry of Education, University and Research (MIUR) for PRIN Funds 2008LYSEBR. We also thank CILEA (Consorzio Interuniversitario Lombardo Elaborazione Automatica) for use of their supercomputers. Finally, we thank University of Brescia for granting a special fund for international collaboration.

REFERENCES

(1) Mc Donagh, A. F. Bile Pigments: Bilatrienes and 5,15-Biladienes. In *The Porphyrins*; Dolphin, D., Ed; Academic Press: New York, 1979; Vol. 6, p 293.

(2) Schmid, R.; McDonagh, A. F. Hyperbilirubinemia. In *The Metabolic Basis for Inherited Diseases*; Stanbury, J. B., Wyngaorder, J. B., Frederickson, D. S., Eds.; McGraw-Hill: New York, 1978; pp 1221−1257.

(3) Bonnett, R.; Davies, J. E.; Hursthouse, M. B.; Sheldrick, G. M. *Proc. R. Soc. London B* **1978**, *202*, 249−268.

(4) LeBas, C.; Allegret, A.; Mauguen, Y.; De Rango, C; Bailly, M. *Acta Crystallogr. B* **1980**, *B36*, 3007−3011.

(5) Kaplan, D.; Navon, G. *Israel J. Chem* **1983**, *23*, 177−186.

(6) Dörner, T.; Knipp, B.; Lightner, D. A. *Tetrahedron* **1997**, *53*, 2697−2716.

(7) Berova, N.; Nakanishi, K. Exciton Chirality Methods: Principles and Applications. In *Circular Dichroism: Principles and Applications*, 2nd ed.; Berova, N., Nakanishi, K., Woody, R. A., Eds.; Wiley-VCH: New York, 2000.
(8) Person, R. V.; Peterson, B. R.; Lightner, D. A. *J. Am. Chem. Soc.* **1994**, *116*, 42−59.
(9) Boiadjiev, S. E.; Lightner, D. A. *J. Am. Chem. Soc.* **2000**, *122*, 378−383.
(10) Boiadjiev, S. E.; Lightner, D. A. *Chirality* **2001**, *13*, 251−257.
(11) VCD, General References: (a) Stephens, P. J. In *Computational Medicinal Chemistry for Drug Discovery*; Bultinck, P., de Winter, H., Langenaecker, W., Tollenaere, J., Eds.; Marcel Dekker: New York, 2003; Chapter 26, pp 699−725. (b) Stephens, P. J.; Devlin, F. J.; Pan, J. J. *Chirality* **2008**, *20*, 643−663. (c) Nafie, L. A.; Freedman, T. B. In *Circular Dichroism: Principles and Applications*; Nakanishi, K., Berova, N., Woody, R. W., Eds.; Wiley-VCH: New York, 2000; Chapter 4, pp 97−132. (d) Keiderling, T. A. In *Circular Dichroism: Principles and Applications*; Nakanishi, K., Berova, N., Woody, R. W., Eds.; Wiley-VCH: New York, 2000; Chapter 22, pp 621−666. (d) Polavarapu, P. L.; Zhao, C. *Fresenius' J. Anal. Chem.* **2000**, *366*, 727−734.
(12) VCD, Computational Methods: (a) Stephens, P. J. *J. Phys. Chem.* **1985**, *89*, 748−751. (b) Stephens, P. J.; Lowe, M. A. *Annu. Rev. Phys. Chem.* **1985**, *36*, 213. (c) Buckingham, A. D.; Fowler, P. W.; Galwas, P. A. *Chem. Phys.* **1987**, *112*, 1. (d) Stephens, P. J.; Devlin, F. J.; Chabalowski, C. F.; Frisch, M. J. *J. Phys. Chem. A* **1994**, *98*, 11623. (e) Cheeseman, J. R.; Devlin, F. J.; Frisch, M. J.; Stephens, P. J. *Chem. Phys. Lett.* **1996**, *252*, 211. (f) Stephens, P. J.; Ashvar, C. S.; Devlin, F. J.; Cheeseman, J. R.; Frisch, M. J. *Mol. Phys.* **1996**, *89*, 579−594. (g) Nicu, V. P.; Neugebauer, J.; Wolff, S. K.; Baerends, E. J. *Theor. Chem. Acc.* **2008**, *119*, 245−263. (h) Andrushchenko, V.; Bouř, P. *Chirality* **2010**, *22*, E96−E114.
(13) Stephens, P. J.; McCann, D. M.; Devlin, F. J.; Smith, A. B., III. *J. Nat. Prod.* **2006**, *69*, 1055−1064.
(14) Bergueño-Tapia, E.; Joseph-Nathan, P. *Phytochemistry* **2008**, *69*, 2251−2256.
(15) Abbate, S.; Ciogli, A.; Fioravanti, S.; Gasparrini, F.; Longhi, G.; Pellacani, L.; Rizzato, E.; Spinelli, D.; Tardella, P. A. *Eur. J. Org. Chem.* **2010**, 6193−6199.
(16) Abbate, S.; Burgi, L. F.; Castglioni, E.; Lebon, F.; Longhi, G.; Toscano, E.; Caccamese, S. *Chirality* **2009**, *21*, 436−441.
(17) Goncharova, I.; Urbanová, M. *Tetrahedron: Asymmetry* **2007**, *18*, 2061−2068.
(18) Goncharova, I.; Urbanová, M. *Anal. Bioanal. Chem.* **2008**, *392*, 355−1365.
(19) Goncharova, I.; Urbanová, M. *Anal. Biochem.* **2009**, *392*, 28−36.
(20) Alagona, G.; Ghio, C.; Monti, S. *Phys. Chem. Chem. Phys.* **2000**, *2*, 4884−4890.
(21) Granucci, G.; Mazzoni, M.; Persico, M.; Toniolo, A. *Phys. Chem. Chem. Phys.* **2005**, *7*, 2594−2598.
(22) Metzroth, T.; Lenhart, M.; Gauss, J. *Appl. Magn. Reson.* **2008**, *33*, 457−467.
(23) Boiadjiev, S. E.; Person, R. V.; Puzicha, G.; Knobler, C.; Maverick, E.; Trueblood, K. N.; Lightner, D. A. *J. Am. Chem. Soc.* **1992**, *114*, 10123−10133.
(24) Puzicha, G.; Pu, Y.-M; Lightner, D. A. *J. Am. Chem. Soc.* **1991**, *113*, 3583−3592.
(25) Frisch, M. J.; Trucks, G. W.; Schlegel, H. B.; Scuseria, G. E.; Robb, M. A.; Cheeseman, J. R.; Scalmani, G.; Barone, V.; Mennucci, B.; Petersson, G. A.; Nakatsuji, H.; Caricato, M.; Li, X.; Hratchian, H. P.; Izmaylov, A. F.; Bloino, J.; Zheng, G.; Sonnenberg, J. L.; Hada, M.; Ehara, M.; Toyota, K.; Fukuda, R.; Hasegawa, J.; Ishida, M.; Nakajima, T.; Honda, Y.; Kitao, O.; Nakai, H.; Vreven, T.; Montgomery, J. A., Jr.; Peralta, J. E.; Ogliaro, F.; Bearpark, M.; Heyd, J. J.; Brothers, E.; Kudin, K. N.; Staroverov, V. N.; Kobayashi, R.; Normand, J.; Raghavachari, K.; Rendell, A.; Burant, J. C.; Iyengar, S. S.; Tomasi, J.; Cossi, M.; Rega, N. ; Millam, J. M.; Klene, M.; Knox, J. E.; Cross, J. B.; Bakken, V.; Adamo, C; Jaramillo, J.; Gomperts, R. E.; Stratmann, O.; Yazyev, A. J.; Austin, R.; Cammi, C.; Pomelli, J. W.; Ochterski, R.; Martin, R. L.; Morokuma, K.; Zakrzewski, V. G.; Voth, G. A.; Salvador, P.; Dannenberg, J. J.; Dapprich, S.; Daniels, A. D.; Farkas, O.; Foresman, J. B.; Ortiz, J. V.; Cioslowski, J.; Fox, D. J. *Gaussian 09*, Revision A.02; Gaussian, Inc.: Pittsburgh, PA, 2009.
(26) Brower, J. O.; Huggins, M. T.; Boiadjiev, S. E.; Lightner, D. A. *Monatsh. Chem.* **2000**, *131*, 1047−1053.
(27) Boiadjiev, S. E.; Lightner, D. A. *J. Heterocyclic Chem.* **2000**, *37*, 863−870.
(28) Furche, F.; Ahlrichs, R.; Wachsmann, C.; Weber, E.; Sobank, A.; Vögtle, F.; Grimme, S. *J. Am. Chem. Soc.* **2000**, *122*, 1717−1724.
(29) Yamay, T.; Taw, D. P.; Handy, N. *Chem. Phys. Lett.* **2004**, *393*, 51−57.
(30) Bauman, D.; Killet, C.; Boiadjiev, S. E.; Lightner, D. A.; Schönhofer, A.; Kuball, H. G. *J. Phys. Chem.* **1996**, *100*, 11546−11558.
(31) Kaplan, D.; Navon, G. *Biochem. J.* **1982**, *201*, 605−613.
(32) Zhang, P.; Polavarapu, P. L. *J. Phys. Chem. A* **2007**, *111*, 858−871.
(33) Yang, B.; Taylor, R. C.; Morris, M. D.; Wang, X.-Z.; Wu, J.-G.; Yu, B.-Z.; Xu, G.-X.; Soloway, R. D. *Spectrochim. Acta* **1993**, *49A*, 1733−1749.